
An experimental investigation towards calibration of a shock tube and stagnation heat flux determination

Sumit Agarwal and Niranjan Sahoo*

Department of Mechanical Engineering,
Indian Institute of Technology Guwahati,
Assam-781039, India
Fax: 0091-361-258-2699
Email: sumit.agarwal@iitg.ernet.in
Email: shock@iitg.ernet.in
*Corresponding author

Abstract: This paper aims at comprehensive investigations towards design and installation of a moderate size shock tube (7 m long having an inner diameter of 55 mm, 20 mm thickness) and its experimental calibration through comparative parametric study. Necessary instrumentations are incorporated for measuring shock speeds and pressure rise across primary as well as reflected shock, obtained using nitrogen/helium as driver gas. The experimental evidence shows reasonable agreement between theoretical (one-dimensional shock tube relations) results. Further, an E-type coaxial surface junction thermocouple (CSJT) has been prepared in the laboratory and oil-bath calibration experiment gives its 'sensitivity'. Measurement of instantaneous surface temperature rise and subsequent stagnation heat flux are obtained using CSJT mounted on a specially-designed end-flange. The thermocouple noted a maximum rise of temperature of 7,800 K, marked as a characteristic constant of the sensor; since it is found to be independent of the magnitude of the step change in temperature.

Keywords: shock tube; primary shock; reflected shock; coaxial surface junction thermocouple; CSJT; stagnation heat flux.

Reference to this paper should be made as follows: Agarwal, S. and Sahoo, N. (2018) 'An experimental investigation towards calibration of a shock tube and stagnation heat flux determination', *Int. J. Aerodynamics*, Vol. 6, No. 1, pp.18–40.

Biographical notes: Sumit Agarwal received his Bachelor's degree (BE) in Mechanical Engineering from the Gauhati University in 2011. Currently, he has been enrolled as a doctorate student in the Department of Mechanical Engineering, Indian Institute of Technology Guwahati since 2012. His broad areas include design and development of thermal sensors, aero test facilities and its instrumentation, heat transfer measurement, measurements in a gas turbine.

Niranjan Sahoo received his PhD degree in Aerospace Engineering from the Indian Institute of Science, Bangalore, India in the year 2004. Currently, he has been working as a Professor in the Department of Mechanical Engineering, Indian Institute of Technology Guwahati. His broad areas of research include dual-fuel combustion, renewable energy, fluid dynamics, experiments in fluids and high-speed aerodynamics.

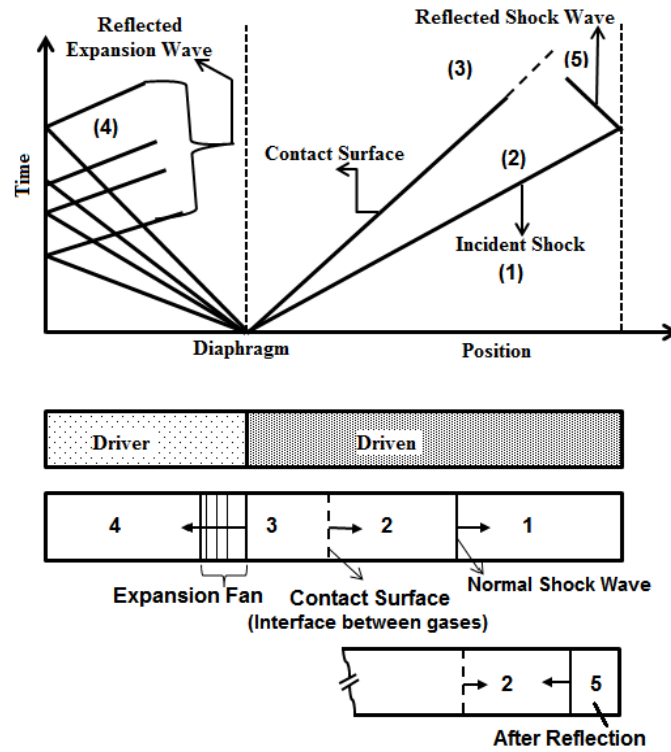
1 Introduction

Shock waves are considered to be an integral part of flow field features in the area of high-speed aerodynamics. In the middle of the eighteenth century, after a series of studies and experiments, it was realised that the waves from explosions travel faster than the speed of the sound waves. Later, shock tubes are fabricated from low-cost materials that can produce pressure pulses through explosives (Duff and Blackwell, 1966). The phenomena of shock wave carry a significant amount of energy and they have the ability to propagate in conventional mediums (solid, liquid and gas) as well as through plasma and electromagnetic field. It further leads to compression of the medium that can change the properties of the medium drastically. The capability of shock waves to generate an instantaneous rise in pressure and temperature pulses in the medium suits its usage in many research areas of space engineering, high-temperature materials, chemical kinetics, medical and industrial applications. With respect to the aerodynamic point of view, the high speed and high altitude flows were simulated by using conventional facilities such as supersonic/hypersonic wind tunnel. With the realisation of shock wave capabilities, high enthalpy short duration impulse facilities came into existence to understand the problem of re-entry and scramjet engines. But, due to lack of high-speed sensors and flow diagnostic instrumentation, these facilities provided limited data. With recent developments in high-speed data acquisition, it is possible to generate hypersonic flows by using a moderate size impulse facility for very short time duration with the test time of few milliseconds. Although there are difficulties in the processing of data acquisition for short test times, the modern high-speed instrumentations and flow diagnostics techniques enable required solution for the intended time duration. Based on these concepts, many impulse test facilities involving large and small-scale shock tunnels, free-piston shock tunnel and expansion tubes have been developed over last few decades (Modarres and Azzazy, 1988; Doolana and Morgan, 1999; Itoh et al., 2001; Stalker et al., 2005). They can provide a high-enthalpy slug of test gas at a very reasonable cost, which is considered as the main attraction in the above developments.

A shock tube is the simplest form of device that can generate moving shock waves by allowing a high-pressure region to suddenly come in contact with a low-pressure region. Basically, it is a closed tube having a driver (region '4') and driven section (region '1') separated by a diaphragm (Figure 1). Both sections have substantially different fill pressures so that the diaphragm opens suddenly, at a point depending on the rupture pressure of the material. Typically, shock tubes are fabricated from stainless steel while diaphragms are made out of cellophane, aluminium, or steel etc. depending on the strength of shock wave requirement. Thus, the gas from the high pressure (driver) section expands into the low pressure (driven) section of the tube, which contains the test gas. On the sudden rupture of the diaphragm, pressure waves originating from the diaphragm section coalesce to form the shock front, which propagates into the low-pressure section. It is known as 'primary shock' which followed by a 'contact surface' which is an imaginary line acting as an interface between the driven and driver gases (regions '2' and '3') in the medium (Figure 1). The moving primary shock travelling towards a driven section of the shock has a velocity greater than the sonic velocity of the undisturbed test gas. It leads to compression, heating and accelerating the test gas for which there is a sudden rise in pressure and temperature (region '2') as shown in Figure 1. The shock wave typically has a thickness of a few microns across which the compressed medium

reaches its equilibrium values of pressure, density and temperature at this distance. Upon reaching the end of the tube, the incident primary shock wave reflects and travels backward. At this point, the test gas has acquired the properties corresponding to region '2'. Immediate upon the reflection from the end of the driven section, the gas particles have zero velocity so that the test gases are modelled as a slug of 'stagnant gas' for a very short test time (Takayama et al., 2014). Subsequently, when the reflected shock travels backward, the medium (test gas) is further compressed and heated (region '5'). On the other side of the diaphragm location, series of expansion waves are initiated upon rupture of the diaphragm. They propagate towards driver section of the tube and get reflected from the end wall of the high-pressure section (Takayama et al., 2014). Thus, the appropriate length ratio of the driver and the driven section is maintained so that driver gases do not contaminate the test gases during test flow durations. The test medium (i.e., modelled as a slug of mass) under sudden compressed and heated conditions (regions '2' and '5') invites many interesting mechanical applications in the areas of chemical kinetics (Bhaskaran and Roth, 2002), ignition delay measurements for fuels (Spadaccini and Colket, 1994), impact assessment on structures (Andreotti et al., 2015) and shock assisted deformation studies (Ray et al., 2015).

Figure 1 Schematic representation of a conventional shock tube and its working principle



In this backdrop, the present investigations are aimed at the development of a modular-type moderate size shock tube suited for a variety of interdisciplinary applications. An in-house developed coaxial surface junction probe (e-type thermocouple) has been fitted in the driven section end flange of the shock tube to determine the stagnation heat flux. Essentially, mounting of the thermocouple on the end flange would suddenly expose it to a high temperature bath created behind the reflected shock during operation of the shock tube. Such an exposure of a thermal sensor to step change in temperature is possible only in few devices like shock tube. By creating a high temperature bath for very short duration can be utilised not only for measurement of stagnation heat flux but also for calibration of the thermal sensor. Hence, one can find out the maximum rate of temperature rise which it can sense by any thermal sensors. In view of this fact, a shock tube (7 m long) is considered with stainless steel that has of 55 mm inner diameter and thickness of 11 mm. This paper depicts a complete investigation towards design details of different components along with necessary instrumentation. The calibration methodologies have been discussed in a comprehensive and systematic manner. Subsequently, an e-type coaxial surface junction thermocouple mounted on the end flange of the shock tube has been used to measure the stagnation heat flux.

2 Design and fabrication methodology for shock tube

One of the fundamental objectives of this investigation is to install a moderate size unique shock tube facility. Some of the major milestones of this facility development are to find the suitable geometrical parameters of the shock tube followed by its fabrication with allied hardware, sophisticated instrumentation for acquiring experimental data and calibration for its capabilities.

2.1 Geometric parameters for the shock tube

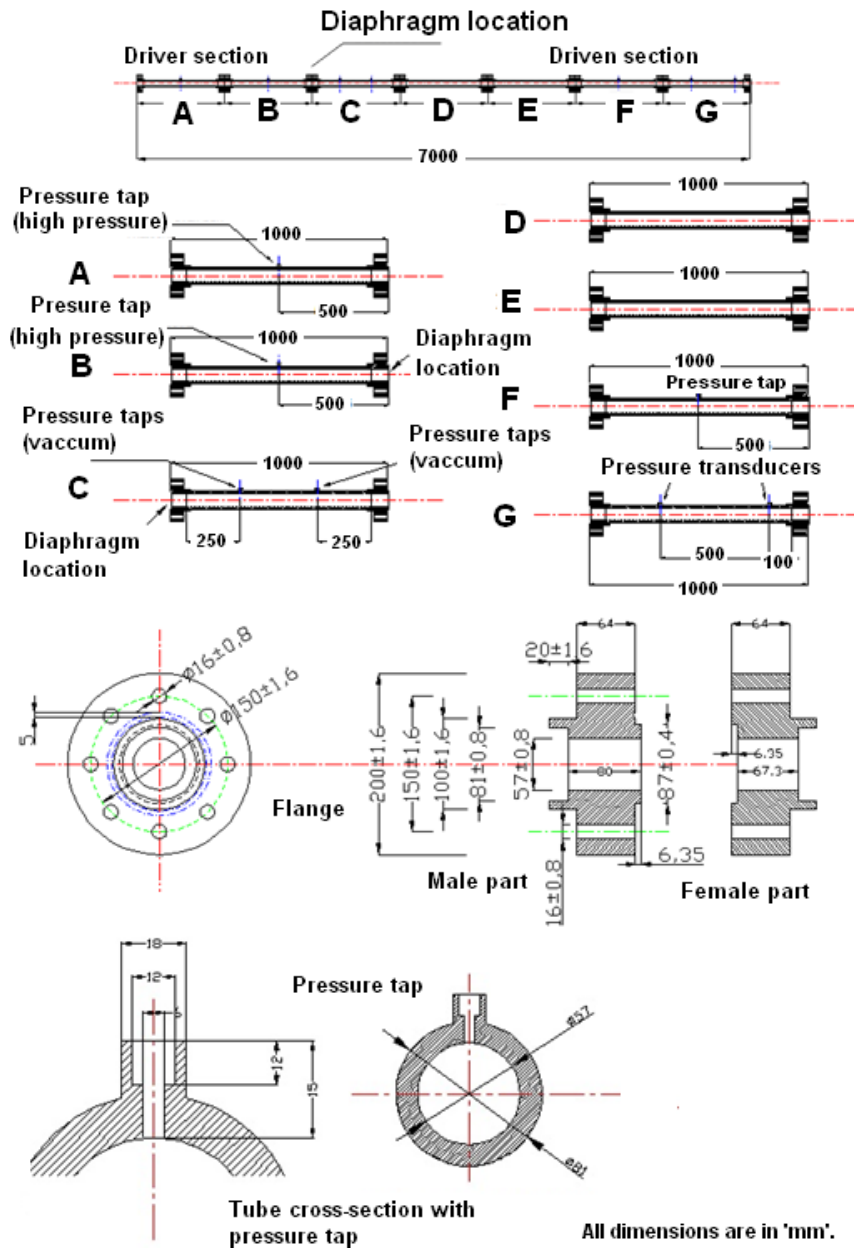
A shock tube normally handles very high pressures for a short test time. So, it is always preferred to study the transient structural behaviour of the material under typical operating conditions. It may be modelled as a generic slug of gas being compressed by shock wave formation and subsequently inducing stresses on the inner wall of the tube. The theory of thin wall pressure vessel can be applied here to estimate ‘hoop stress’ that acts in the circumferential direction (Timoshenko et al., 1956). A spherical vessel of inner radius r and thickness t , when experiences an internal pressure p_i , can be considered as a thin walled vessel, when $r_i / t \geq 10$. Such a vessel is known as a shallow-walled pressure vessel for which ‘hoop stress (σ_h)’ is given by the following expression:

$$\sigma_h = \frac{p_i r_i}{2t} \quad (1)$$

In this case, stainless steel tubes are considered (density: 7,900 kg/m³; elastic modulus: 193 GPa; yield strength: 240 MPa and Poisson’s ratio: 0.3) with 55 mm inner diameter and thickness of 11 mm (Cobb, 2010). The internal pressure is considered as 25 bar,

which is kept as the upper limit of the operating condition of driver gas pressure during rupture of the metallic diaphragm. In order to ensure the fact that expansion waves do not interfere the test slug gases, the lengths of the driven section are considered as a longer tube of 5 m long. All the geometrical parameters for the assembly of shock tube and its part component are shown in Figure 2.

Figure 2 Design and geometrical parameters for shock tube assembly (see online version for colours)



2.2 Installation of shock tube

The shock tube is constructed from stainless steel of 1 m long tube with driver section having two tubes and a driven section with five tubes. The longer driven section ensures the fact that the attenuation of the shock fronts does not become a major factor when it is reflected from the end wall. The inner diameter of the tube is 55 mm with a thickness of 11 mm. A metallic diaphragm mounted on the flange separates the driver and driven sections of the tube. Aluminium sheet with a diameter of 100 mm, thickness 1.2 mm is used to fabricate the diaphragms for the shock tube (Figure 3). In order to have a controlled rupture of diaphragm and generation of the shock wave, V-grooves are made with one-third of the total thickness of diaphragm (Takayama et al., 2014). It ensures the fact of localised rupture at the point with lowest stress concentration factor (Timoshenko et al., 1956). To the best possible extent, the uniformity of rupture pressure will be maintained when a particular thickness of the diaphragm is chosen. Moreover, the inherent impurities in the material will not affect significantly to the rupture pressure. The driver section consists of high-pressure gas, pressure regulator, pressure gauges (analogue and digital) with adequate number valves for regulation of gas. It is of two-meter length to which the high-pressure gas enters through a ball valve. The gas cylinder is attached to pressure regulator so that the pressure inside the driver section and mass flow rate of the gas can be easily controlled. At the opening of the cylinder, two ball valves are placed; one for the entry of the high-pressure gas inside the cylinder and other for the discharge of gas from the cylinder to the atmosphere. The driven section of the shock tube (with 5 m long) has the components vacuum pump (rotary type; ED6 series; HHV Pumps Private Ltd., Bangalore), vacuum gauge and a U-tube-manometer. In the first tube of the driven section, there are two openings, one for the connection to the vacuum pump so that low pressures can be created inside the driven section and another is connected to vacuum pressure gauge and U-tube manometer. In order to check the repeatability of the vacuum gauge, the U-tube manometer is connected via a T-joint. The fourth and fifth tubes are fully closed while there are provisions of placing pressure transducers and thermal sensors. The overview of all the instrumentations and data reduction techniques of shock tube operation is shown in the line diagram (Figure 4).

Figure 3 Design of metallic diaphragm for shock tube experiments

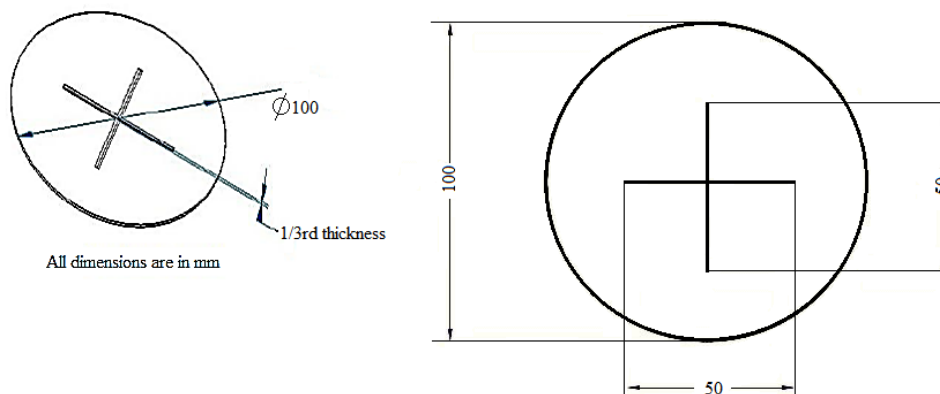
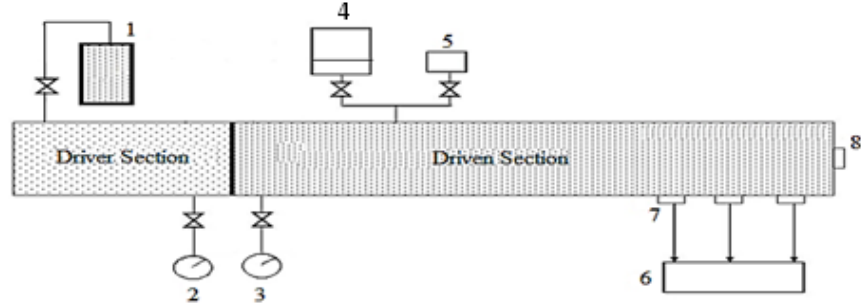


Figure 4 Line diagram of shock tube with different components and its operation

Notes: 1: high pressure gas cylinder; 2: high pressure gauge; 3: vacuum gauge; 4: vacuum pump; 5: U-tube manometer; 6: oscilloscope; 7: pressure sensor; 8: thermocouple.

2.3 Instrumentation for the shock tube

In the entire process of calibration and experiments in a shock tube, there are certain prime requirements such as maintaining appropriate pressure ratios across the diaphragm (i.e., between the driver and driven section), measuring shock speed and pressure rise across the shock waves. The driver side pressure (p_4) is monitored on the control console through a high-pressure gauge mounted pressure tap. The driven section initial pressure (p_1) is obtained through parallel measurements from a precision vacuum gauge as well as a mercury manometer. The temperatures in the driver and driven sections (T_1 and T_4) are considered as room temperature of 25°C. Two pressure transducers (PCB piezotronics, USA; model 113B22) are mounted at the locations of pressure taps in the last segment of driven side of the shock tube (Figure 5). A stainless steel holder (1/4" BSP thread) used over 10.8 mm length (approximately equal to the thickness of shock tube) houses the pressure transducers, thereby flush mounted with inner tube surface. The pressure sensor mounted in flush with the inner surface of the shock tube, measure the pressure jump behind primary as well as reflected shock waves due to rupture of the diaphragm. Whenever the primary shock passes over the two sensors, a step change in the voltage signals is seen in the oscilloscope (make: Yokogawa, having a bandwidth of 200 MHz and a sampling rate of 2.5 GS/s), corresponding to pressure jump across the shock wave (region '2'). Subsequently, when the shock waves reflect from the end flange of the driven section, there is further rise in pressure (region '5') because the reflected shocks pass through already elevated medium of higher pressure.

The coaxial surface junction thermocouples (CSJT) are intended to capture stagnation temperature rise across the reflected shocks. In this setup, in-house designed e-type CSJT is installed at the end of the driven tube in a specially designed end-plate attachment made out of stainless steel (Figure 6). In order to mount the thermocouple, in the end-flange, the thermocouple holders are designed so that it can be mounted in flush with the inner surface of the end flange. The material for thermocouple holder is also stainless steel which is similar to the pressure transducer holders. Here, a hole of 6 mm diameter and 9 mm depth is provided to hold the e-type CSJT (Figure 6). Another, 3 mm hole is provided for electrical connection from the sensing element to the amplifier of the

thermocouple. The gap between the thermocouple and holder is filled by wrapping with Teflon on the thermocouple and the sensor gets insulated from the end plate of the shock tube. Normally, CSJT works on the principle of ‘Seebeck effect’ in which a voltage signal is produced corresponding to a temperature change at the surface junction. Thus, for capturing this time varying signal, the CSJT is instrumented with a voltage amplifier (INA 128; Techno Science Instruments; Bangalore) with adequate gain factors.

Figure 5 Design, fabrication of pressure sensor holder and its mountings in the driven section of shock tube (see online version for colours)

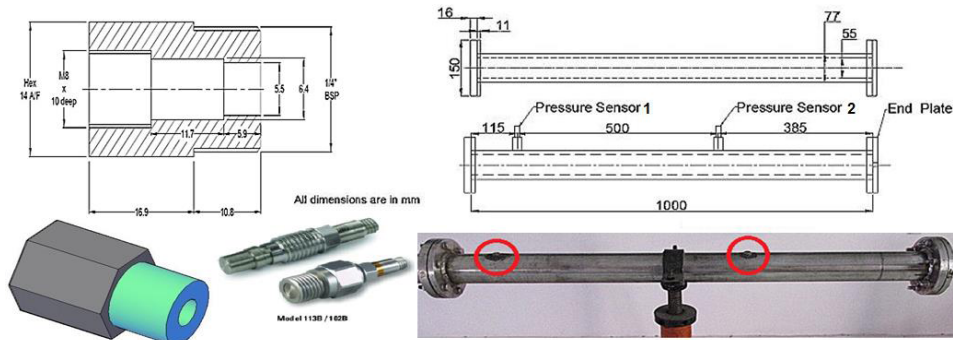
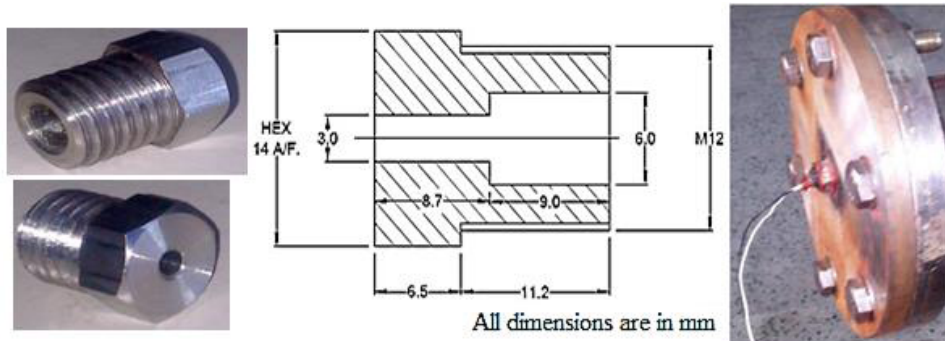


Figure 6 Design and fabrication of thermocouple inserts and its mounting on the endplate of the shock tube (see online version for colours)



3 Calibration of shock tube

The constant area shock tube is a laboratory tool that creates a plane shock wave by the sudden rupture of diaphragm separating the high (driver) and low (driven) pressure region of the tube. When the diaphragm suddenly bursts, the high-pressure gas rushes into the low-pressure test gas. It induces a series of compression and expansion waves that propagate into driven and driver section of the shock tube. The compression waves travelling towards low-pressure region coalesce to form a strong normal shock while a series of expansion waves travel to the high-pressure region (Figure 1). At the same time,

the interface between the test gas and driver gas also travels into the low-pressure section. When the shock wave reaches the end of a tube, it gets reflected from the end flange and travelling back into the driven section. The gas between the shock wave and the interface is the ‘test gas’ with high pressure, temperature and velocity with respect moving slug of the gas column at high temperature and pressure can be treated as momentary ‘impulsive heat/force’ for simulating flow fields over aerodynamic models. However, the test duration for such uniform flow is limited to few milliseconds. Since shock waves can be generated under controlled conditions, many analogous natural occurring phenomena related to shock-associated/shock wave physics can be simulated experimentally by using ‘shock tube’ as a laboratory tool. Because of simplicity and low cost of operations, shock tube is treated as a unique laboratory tool for many other engineering applications as well. Prior to its usage in practical applications, the performance of the shock tube needs is evaluated with respect to its ideal behaviour.

3.1 Shock tube relations

The ideal behaviour of a shock tube is predicted through one-dimensional gas-dynamic relations (Anderson, 2004). Consider the shock tube sketched in Figure 1, where the high-pressure gas having specific heat ratio (γ_4) is separated from low-pressure gas with specific heat ratio (γ_1) by a diaphragm.

$$\frac{p_2}{p_1} = 1 + \frac{2\gamma_1}{\gamma_1 + 1}(M_s^2 - 1); \frac{T_2}{T_1} = \frac{1 + \left(\frac{\gamma_1 - 1}{\gamma_1 + 1}\right) \frac{p_2}{p_1}}{1 + \left(\frac{\gamma_1 - 1}{\gamma_1 + 1}\right) \frac{p_1}{p_2}} \quad (\text{i})$$

$$\frac{p_4}{p_1} = \left(\frac{p_2}{p_1}\right) \left[1 - \frac{(\gamma_4 - 1)(a_1/a_4) \left(\frac{p_2}{p_1} - 1\right)}{(\sqrt{2\gamma_1}) \left(\sqrt{\left(2\gamma_1 + (\gamma_1 + 1) \left(\frac{p_2}{p_1} - 1\right)\right)} \right)} \right]^{\frac{-2\gamma_4}{(\gamma_4 - 1)}} \quad (\text{ii})$$

$$u_2 = u_3; p_2 = p_3; a_1 = \sqrt{\gamma_1 R_1 T_1}; a_4 = \sqrt{\gamma_4 R_4 T_4} \quad (\text{iii})$$

$$\frac{p_5}{p_1} = \left[\frac{2\gamma_1 M_s^2 - (\gamma_1 + 1)}{(\gamma_1 + 1)} \right] \left[\frac{-2(\gamma_1 - 1) + M_s^2 (3\gamma_1 - 1)}{2 + M_s^2 (\gamma_1 - 1)} \right] \quad (\text{iv})$$

$$\frac{T_5}{T_1} = \left(\frac{[2(\gamma_1 - 1)M_s^2 + 3 - \gamma_1][(3\gamma_1 - 1)M_s^2 - 2(\gamma_1 - 1)]}{(\gamma_1 + 1)^2 M_s^2} \right) \quad (\text{v})$$

$$\frac{M_R}{M_R^2 - 1} = \frac{M_s}{M_s^2 - 1} \sqrt{1 + \frac{2(\gamma_1 - 1)}{(\gamma_1 + 1)^2} (M_s^2 - 1) \left(\gamma + \frac{1}{M_s^2} \right)} \quad (\text{vi})$$

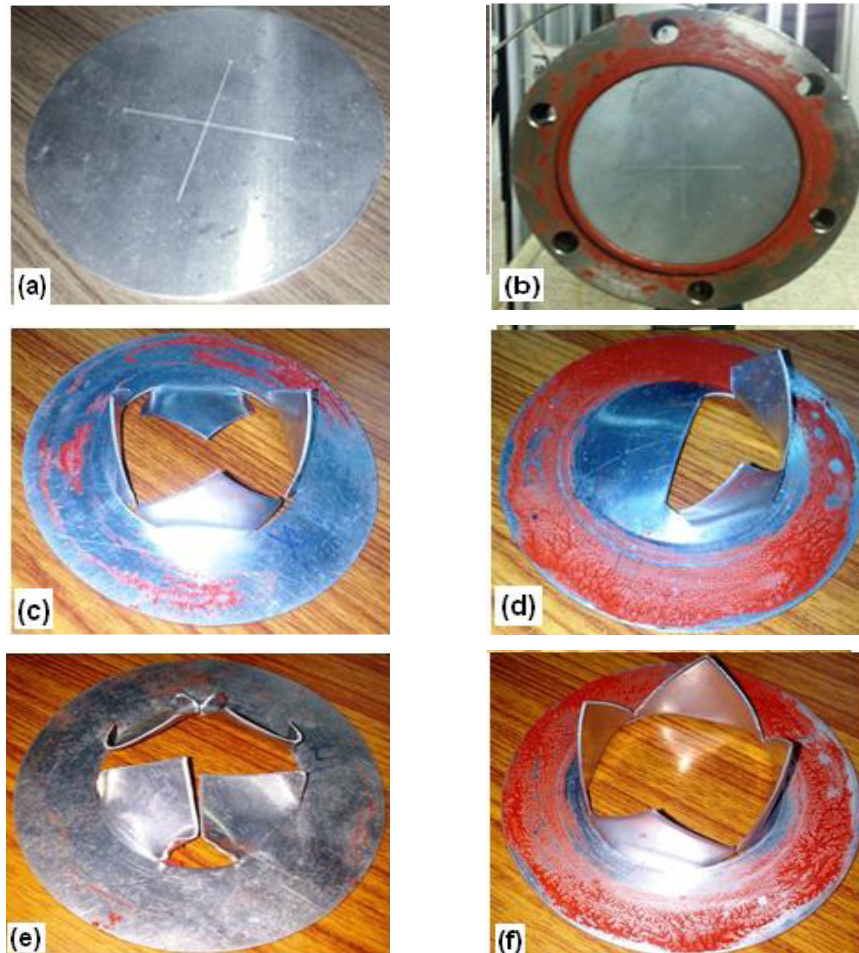
The shock tube’s performance is based entirely upon the pressure ratios (p_4 / p_1) and the ratio of speeds of sound (a_4 / a_1) for driver and driven section. Referring to the notations used for various regions of shock tube at different time instants (Section 1 and Figure 1), the mathematical expressions for calculating pressure and temperature rise across primary

shock (p_2 / p_1 and T_2 / T_1), pressure and temperature rise across reflected shock (p_5 / p_1 and T_5 / T_1) can be expressed as a function of primary shock Mach number (M_s).

3.2 Experimental procedure for shock tube operation

Initially, an aluminium diaphragm of 1.2 mm thickness separates the driver and driven section of the shock tube [Figures 7(a) and (b)]. Since the strength of the shock increases with increase in the ratio of speeds of sound, it is desirable to have a driver gas with a low molecular weight. Conversely, driven gas should have high molecular weight. So, the strongest shock wave is obtained by using a heavy driven gas and a light driver gas. While meeting these requirements, the present investigation is aimed for two driver gases (nitrogen and helium) with air in the driven section of the shock tube (Kore et al., 2016; Nanda et al., 2017).

Figure 7 Diaphragm rupture process in the shock tube (see online version for colours)



At the beginning of the experiment, the pressure inside the driven section (p_1) is maintained at 0.18 bar and all the valves are closed. The driver section (p_4) is filled with nitrogen/helium through a high-pressure cylinder and the diaphragm ruptures at a pressure of 20 bar. The sudden rupture of the diaphragm due to the pressure difference between the driver and driven section of the tube creates a shock wave that propagates into the driven section. The critical factor of designing the V-groove on the diaphragm plays an important role during the rupture process that can be seen in Figure 7. If the diaphragm does not rupture instantaneously, then it leads to the only formation of compression waves [Figures 7(c), (d) and (e)]. Studies have shown that most often the crack in the diaphragm starts at the centre and spreads to the edges (Takayama et al., 2014). Therefore, the gas flow starts as a jet initially followed by a subsequent mass flow of driver gas after the petal-like complete rupture of the diaphragm [Figure 7(f)]. This controlled nature diaphragm rupture often resembles the formation of shock wave because of coalescence of series of compression waves. The sudden rise in pressures across the shock wave induces mass motion of the driven gas (air). The primary shock gets reflected from the end plate, thus forming the reflected shock. The pressure jumps across the primary as well as a reflected shock are captured from the pressure transducers mounted at the last segment of the driven tube in the form of voltage signals. Based on the ‘sensitivity’ information as supplied by the manufacturer, pressure rise across primary and reflected shocks are measured. A typical signal is shown in Figure 8 with helium as driver gas and air as the test gas. With the knowledge of the distance between pressure taps (ΔS), time taken by the shock waves (Δt) to travel this distance (obtained from pressure signals), speed of sound in the ‘region 1’ (a_1), the shock wave velocity (V_s) and experimental shock Mach number ($M_{s,e}$) can be calculated from equation (3).

$$V_s = \frac{\Delta S}{\Delta t}; a_1 = \sqrt{\gamma RT_1}; M_{s,e} = \frac{V_s}{a_1} \quad (3)$$

Figure 8 Pressure rise across primary and reflected shock in the shock tube

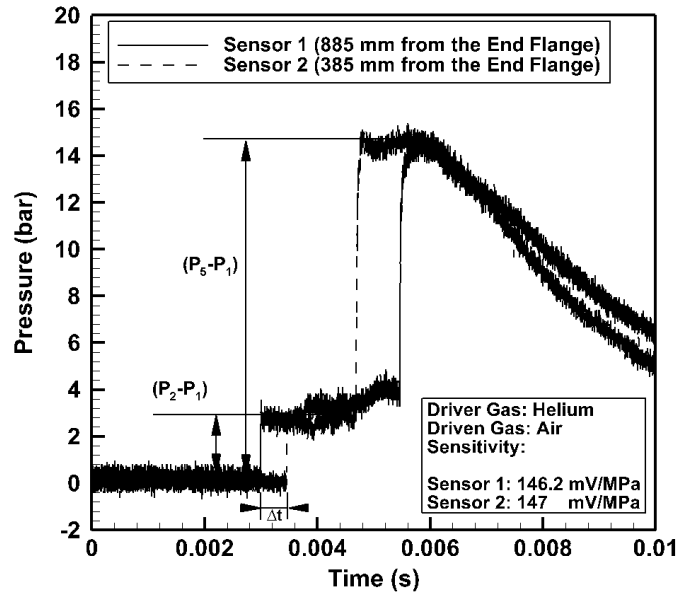
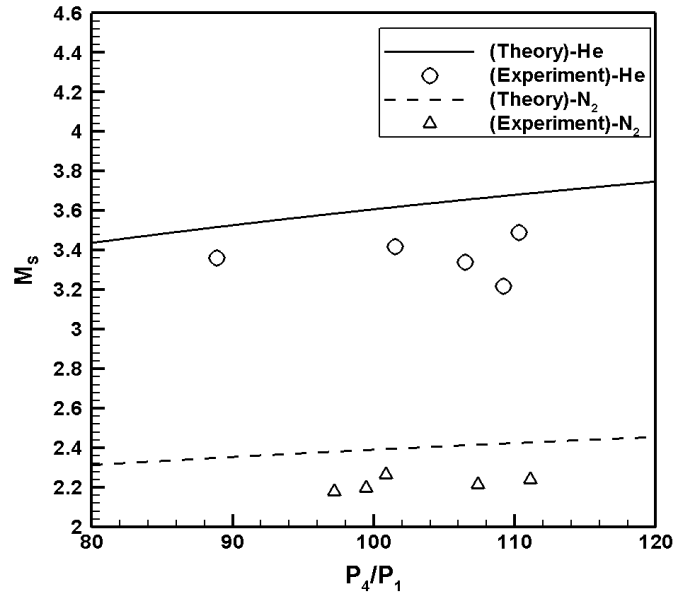


Table 1 Comparison of shock Mach numbers between analytical calculations and experiments

Sl. no.	Driver gas: nitrogen, driven gas: air											
	$p_1 = 0.18 \text{ bar}; \gamma_1 = 1.4; \gamma_4 = 1.4; R_1 = 287 \text{ J/(kg.K)}; R_4 = 297 \text{ J/(kg.K)}$											
	M_s		(p_2 / p_1)		(p_5 / p_1)		(T_2 / T_1)		(T_5 / T_1)			
	Theory ($M_{s,t}$)	Exp ($M_{s,e}$)	Theory (p_2 / p_1) _t	Exp (p_2 / p_1) _e	Theory (p_5 / p_1) _t	Exp (p_5 / p_1) _e	Theory (T_2 / T_1) _t	Exp (T_2 / T_1) _e	Theory (T_5 / T_1) _t	Exp (T_5 / T_1) _e		
1	2.42	2.24	6.66	6.38	27.53	28.31	2.04	1.90	3.34	2.98		
2	2.38	2.17	6.44	6.31	26.16	29.51	2.02	1.84	3.25	2.84		
3	2.39	2.26	6.51	5.85	26.50	22.92	2.03	1.91	3.28	3.01		
4	2.42	2.23	6.69	6.01	27.71	29.06	2.06	1.89	3.35	2.96		
5	2.43	2.26	6.72	6.18	27.85	24.92	2.07	1.91	3.36	3.0		
	Driver gas: nitrogen, driven gas: air											
	$p_1 = 0.18 \text{ bar}; \gamma_1 = 1.4; \gamma_4 = 1.66; R_1 = 287 \text{ J/(kg.K)}; R_4 = 2,077 \text{ J/(kg.K)}$											
6	3.68	3.49	15.63	11.53	89.65	82.84	3.56	3.30	6.78	6.17		
7	3.65	3.34	15.43	8.96	88.14	67.99	3.53	3.10	6.70	5.71		
8	3.52	3.35	14.26	12.50	79.62	76.03	3.33	3.12	6.25	5.76		
9	3.62	3.42	15.11	11.36	85.83	75.92	3.48	3.20	6.58	5.95		
10	3.67	3.22	15.59	16.73	89.34	76.03	3.56	2.95	6.76	5.37		

Figure 9 Comparison of shock Mach numbers (experiment and theory) as a function of pressure ratio (p_4/p_1)**Table 2** Calculation of shock tube parameters with 'nitrogen and helium' as driver gas

<i>Driver gas: nitrogen; driven gas: air</i>						
$p_1 = 0.18 \text{ bar}; \gamma_1 = 1.4; \gamma_4 = 1.4; R_1 = 287 \text{ J/(kg.K)}; R_4 = 297 \text{ J/(kg.K)}$						
p_4 (bar)	(p_4/p_1)	M_s		M_R		
		<i>Theory</i>	<i>Exp</i>	<i>Theory</i>	<i>Exp</i>	
1	19.65	109.17	2.42	2.25	1.97	1.37
2	17.51	97.28	2.38	2.18	1.91	1.35
3	18.13	100.72	2.39	2.26	1.93	1.39
4	19.99	111.05	2.425	2.24	1.98	1.43
5	20.2	112.22	2.429	2.26	1.99	1.41
<i>Driver gas: helium; driven gas: air</i>						
$p_1 = 0.18 \text{ bar}; \gamma_1 = 1.4; \gamma_4 = 1.66; R_1 = 287 \text{ J/(kg.K)}; R_4 = 2,077 \text{ J/(kg.K)}$						
6	19.856	110.31	3.68	3.49	2.25	1.95
7	19.167	106.48	3.65	3.34	2.24	2.29
8	15.995	88.861	3.52	3.36	2.22	1.85
9	18.271	101.51	3.62	3.42	2.24	2.50
10	19.65	109.17	3.67	3.22	2.25	1.76

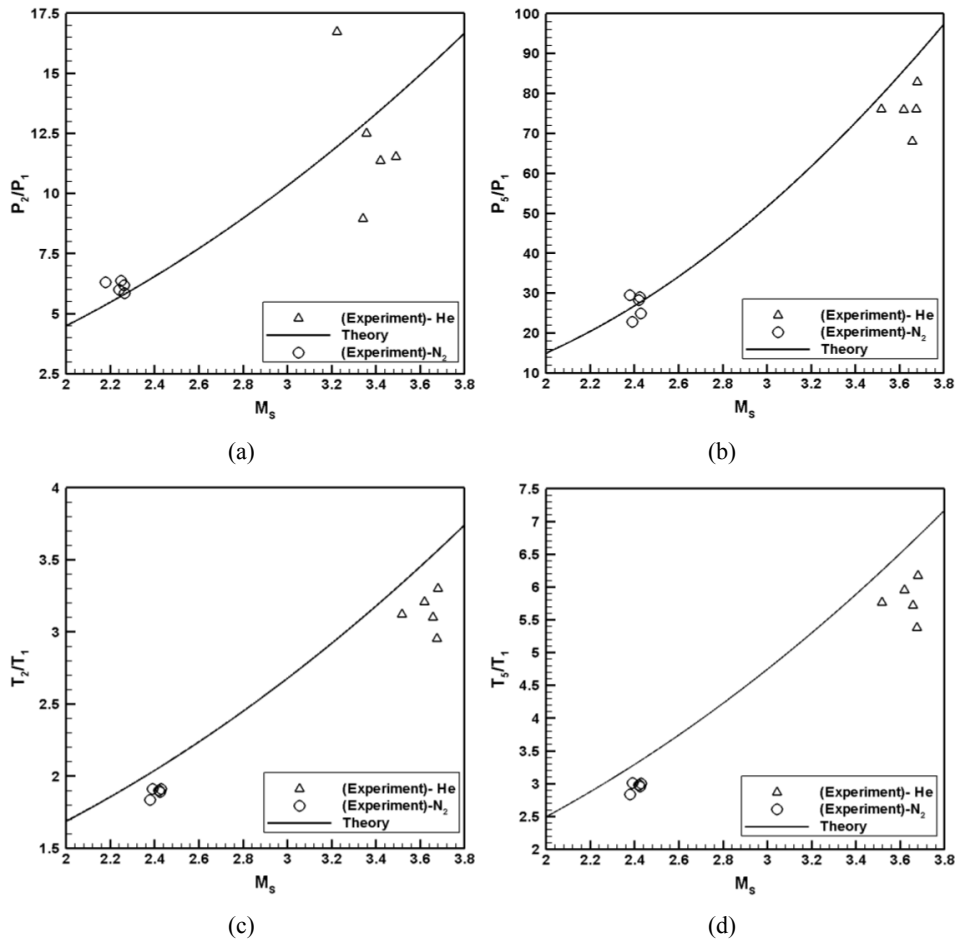
Table 3 Percentage deviation of shock tube parameters during its calibration

Percentage of deviation from theory						
Driver gas: nitrogen						
Sl. no.	$\frac{(M_{s,t} - M_{s,e})}{M_{s,t}}$	$\frac{(p_2/p_1)_t - (p_2/p_1)_e}{(p_2/p_1)_t}$	$\frac{(p_5/p_1)_t - (p_5/p_1)_e}{(p_5/p_1)_t}$	$\frac{(T_2/T_1)_t - (T_2/T_1)_e}{(T_2/T_1)_t}$	$\frac{(T_5/T_1)_t - (T_5/T_1)_e}{(T_5/T_1)_t}$	
Driver gas: nitrogen						
1	7	4.2	-2.8	6.8	10.8	
2	8.4	2	-12.8	8.9	12.6	
3	5.4	10	13.5	5.9	8.2	
4	7.6	10	-4.8	8.2	11.6	
5	6.9	8	10.5	7.7	10.7	
Driver gas: helium						
6	5.1	26	7.6	7.4	9	
7	8.5	41	23	12.2	15	
8	4.5	12	4.5	6.5	7.8	
9	5.5	24	11.5	8	9.5	
10	12.2	-7.3	15	17	20	

Table 4 Uncertainty values for shock tube parameters during calibration

Shock tube parameters	Average value of uncertainty	
	Nitrogen	Helium
M_s	$\pm 0.1\%$	$\pm 0.1\%$
(p_2 / p_1)	$\pm 0.2\%$	$\pm 0.2\%$
(p_5 / p_1)	$\pm 1.6\%$	$\pm 9\%$
(T_2 / T_1)	$\pm 2\%$	$\pm 3\%$
(T_5 / T_1)	$\pm 2.7\%$	$\pm 9\%$
$T_s(t)$	$\pm 0.16\%$	$\pm 0.2\%$
$\dot{q}_s(t)$	$\pm 0.5\%$	$\pm 0.2\%$

Figure 10 Pressure and temperature rise across primary and reflected shocks as a function of shock Mach numbers



Further, the theoretical shock Mach number ($M_{s,t}$) is obtained from initial pressure ratios (p_4 / p_1) across the diaphragm by using equation [2(ii)]. With helium and nitrogen as driver gases (region ‘4’) and air as driven gas (region ‘1’), the comparative assessment of shock Mach numbers ($M_{s,t}$ and $M_{s,e}$) obtained from both the methods (Table 1 and Figure 9). Using the values of $M_{s,t}$ and $M_{s,e}$, one-dimensional shock tube relations [equations 2(i), (iv) and (v)] have been used to compute the theoretical and experimental values of pressure and temperature ratios across primary shock [(p_2 / p_1) and (T_2 / T_1)] and reflected shock [(p_5 / p_1) and (T_5 / T_1)]. These values are calculated for five set of experiments with nitrogen (N_2) and helium (He) as driver gas and the comparative behaviours are given in Table 2 and Figures 10(a) and (b), respectively. Upon reaching the end flange of the driven tube, the shock wave gets reflected at much lower speed. So, with the knowledge of primary shock Mach number ($M_{s,t}$ and $M_{s,e}$), it is also possible to calculate the reflected shock Mach numbers ($M_{R,t}$ and $M_{R,e}$) by using equation [2(vi)]. The values of $M_{R,t}$ and $M_{R,e}$ are given in Table 2 while the trend of the plot is shown in Figure 11. In addition, the percentage of deviation for each of the measured and calculated parameter of the shock tube is illustrated in Table 3. All these calibration curves (Figures 9, 10 and 11) show a reasonably good agreement (within $\pm 12\%$) between the theory and experiments for nitrogen driver. However, the deviation seems to be higher for helium driver in certain test cases, which may be due to its lighter weight and higher shock Mach number (Persico et al., 2005). Since most of the shock tube parameters depend on the square of the shock Mach number, the deviation seems to be amplified. It may also be emphasised that material of the diaphragm and its groove also plays a critical role in the calculation of shock Mach number from the pressure ratio (p_4 / p_1).

Figure 11 Reflected shock Mach number as a function of primary shock Mach number

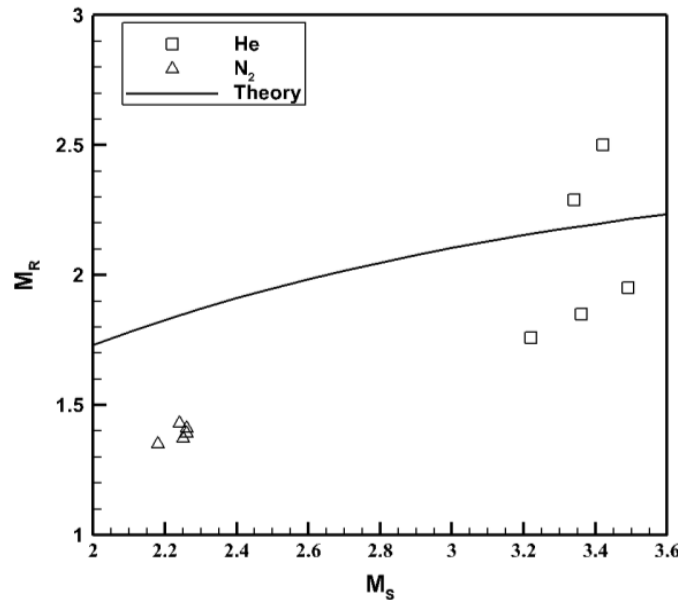
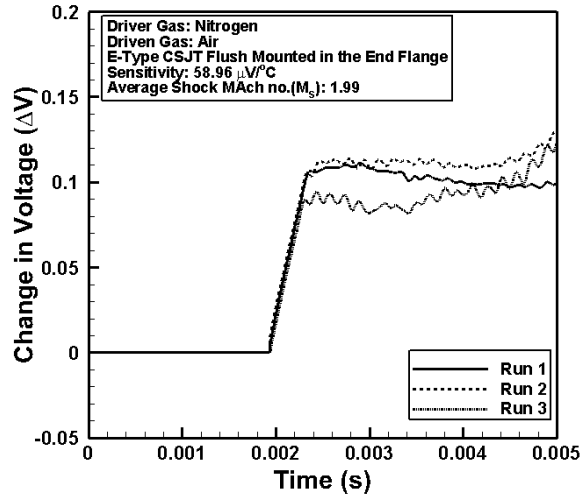
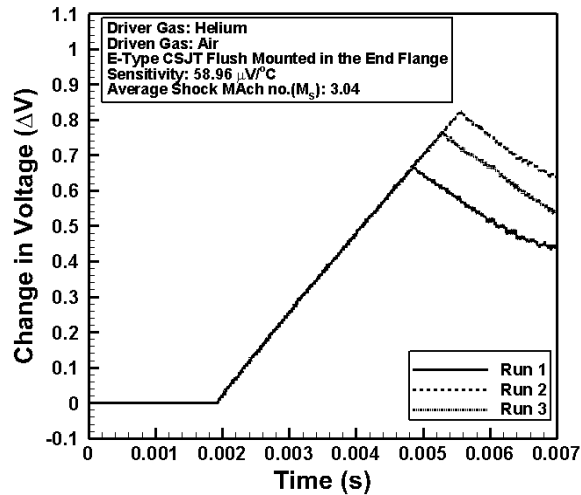


Figure 12 Typical voltage histories captured from CSJT mounted on the end flange of the shock tube obtained using nitrogen and helium as driver gas



(a)



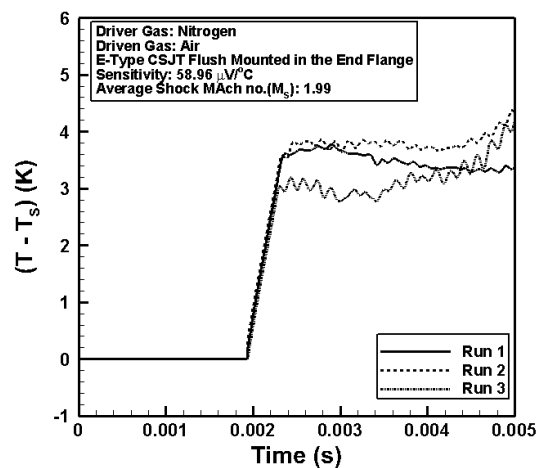
(b)

3.3 Stagnation heat flux measurement in the shock tube

The CSJT are intended to capture the transient rise in temperature across the reflected shocks. In this setup, an e-type CSJT is installed at the end of the driven tube in a specially designed end-plate attachment made out of stainless steel (Figure 6). The e-type CSJT has been prepared in-house with constantan and chromel wires of diameters 0.813 mm and 3.25 mm, respectively. The surface junction is formed by grinding or scratching with abrasive papers or by using file tool, the front surface. Thus, micro-scratches generated by this mechanism make it suitable to respond in short duration time scale. Subsequently, the sensitivity (i.e., a rise in voltage with respect to the rise in temperature)

of CSJT is obtained as, $58.96 \mu\text{V}/^\circ\text{C}$ through standard oil bath calibration. More details of the fabrication method and calibration experiment may be found in the references (Agarwal et al., 2017). In order to mount the CSJT in the end-flange, the thermocouple holders are designed so that it can be fixed in flush with the inner surface of the end flange. During shock tube experiments, the transient rise in temperatures is captured by using the e-type CSJT with nitrogen and helium as driver gases. The typical voltage-time histories and rise in temperatures $[T_s(t)]$ for four different tests are plotted in Figures 12–14. The surface temperature history resembles nature of ‘ramp’, with the rise in temperature of 4°C and 25°C , for nitrogen and helium driver, respectively. From this plot, the temperature gradient ($\Delta T_s / \Delta t$) can be calculated as $7,941 \text{ K/s}$ and $7,679 \text{ K/s}$ with for nitrogen and helium driver, respectively. Thus, the in-house designed thermocouple is found to be capable to respond a very high rate of temperature rise. Contrarily, rate of temperature rise felt by the sensor during static calibration is very small (Taler, 1996). Further, it is interesting to see that the rate of temperature rise is almost same in experiments with nitrogen and helium drivers. As noted from the data in Table 1, the expected temperature behind the reflected shock for nitrogen driver is 900 K while for helium driver this value is approximately $1,800 \text{ K}$. During experiments, Further, the transient responses from the thermocouples (Figures 13 and 14) depict the fact that the rate of temperature rise is independent of step height i.e. the rate of rise of temperature signal is in same for both nitrogen and helium driver. After the sudden rise in temperature, in both the signals (Figures 13 and 14), there is change in slope of the temperature signal. In case of nitrogen driver, rate of rise decreases while in case of helium driver, rate of rise becomes negative. These alterations in the temperature signal are indications of end of the test time in the shock tube and arrival of multiple waves and their complicated interactions. Further, the occurrence of any interaction between different waves depends upon the shock tube driving conditions, which is accounted for change in pattern of the temperature signals. The interpretation of such phenomena through temperature signals from surface junction thermocouples is one of the strong outcomes of this experimental investigation.

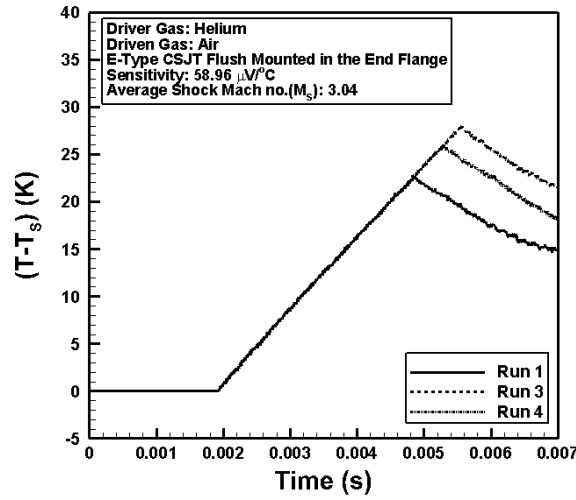
Figure 13 Typical rise in transient surface temperature captured from CSJT mounted on the end flange of the shock tube obtained using nitrogen as driver gas



These temperature signals are then used for evaluating the respective stagnation heat flux. Here, thermal properties of the substrate are treated as constant and the surface heat flux $\dot{q}_s(t)$ is calculated by using Duhamel's superposition integral as given below (Agarwal et al., 2017),

$$q_s(t) = \frac{\beta}{\sqrt{\pi}} \int_0^t \frac{d\{T_s(t)\}}{dt} \frac{1}{\sqrt{t-\tau}} d\tau \quad (4)$$

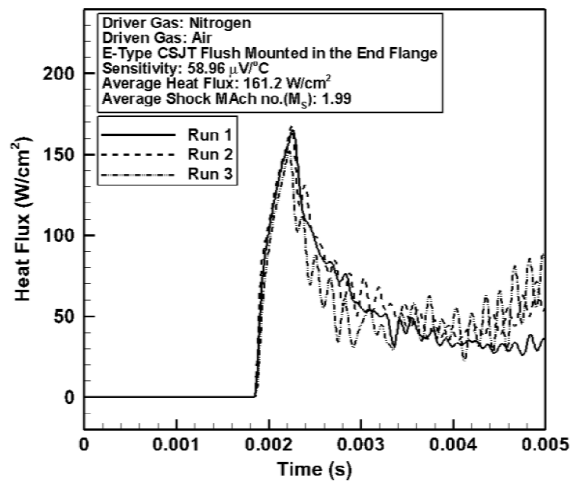
Figure 14 Typical rise in transient surface temperature captured from CSJT mounted on the end flange of the shock tube obtained using helium as driver gas



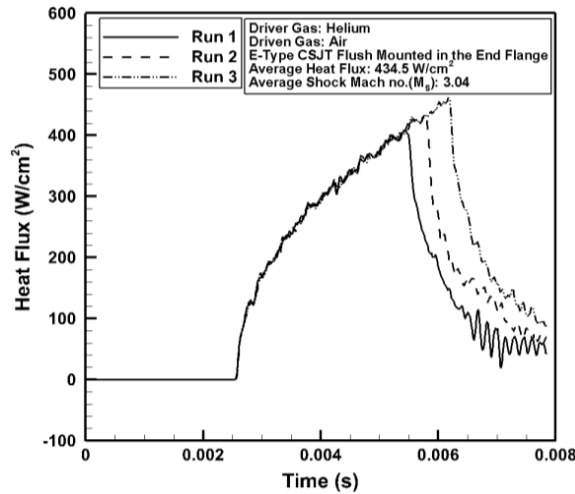
The polynomial equation using cubic-spline method is used in the present work to discretise the temperature data $[T_s(t)]$ for obtaining a closed form solution. More details of discretisation techniques are available in the references (Agarwal et al., 2017). In order to use equation (4), it is desired to have closed form solution of transient temperature data and estimation of the thermal product ($\beta = \sqrt{\rho ck}$), where ρ , c and k are the density, specific heat and thermal conductivity of the thermocouple material, respectively. For co-axial thermocouples, the thermal properties mainly depend on the materials by which the surface junction is formed. Since the surface of the junction is made with two different metals, it is appropriate to use weighting factor 0.5 each thermocouple metallic element and the value of β is calculated by the methods given in the references (Shultz and Jones, 1973; Mohammed et al., 2008; Menezes and Bhat, 2010). At room temperature of 300 K, the value of β is obtained as $8,300 \text{ J/m}^2\text{s}^{0.5}\text{K}$. The surface heat flux computed by using equation (4) for all the tests (nitrogen and helium driver) are plotted in Figure 15. A typical comparison of heat flux signals for helium and nitrogen driver is shown in Figure 16. Similar trends of surface heat flux are seen with different peak heat flux values as, 160 W/cm^2 and 434 W/cm^2 , with nitrogen and helium driver gas, respectively. This 'similarity nature' in the heat flux signal can be marked as the property of the sensor since the maximum rate of temperature rise is same for both driving

conditions. Further, different interactions may be responsible for the change in heat flux signal after the test time. Thus, present studies are found essential in evaluating the maximum rate of temperature rise for a given thermal sensor, thus considered as the property of sensing surface. In this case, the CSJT fabricated in-house has a potential of capturing highly transient phenomena of temperature rise in a shock tube. With another view point, current investigations also recommend the use of shock tube as calibrating facility of any transient thermal sensors for evaluating the maximum rate of temperature rise.

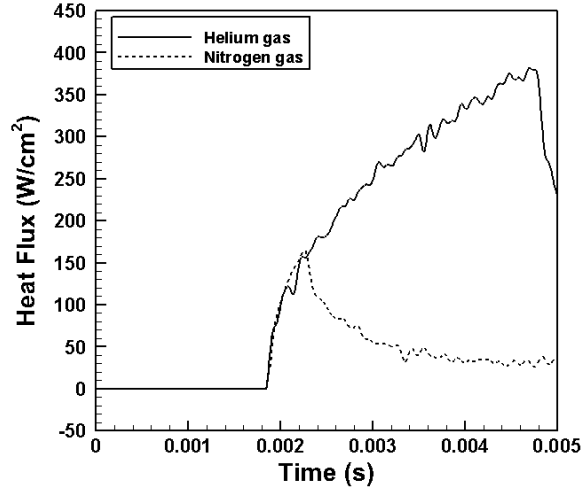
Figure 15 Surface heat flux histories obtained through one-dimensional heat conduction modelling from temperature histories of CSJT, mounted on the end flange of the shock tube



(a)



(b)

Figure 16 Comparison of surface heat flux obtained using both helium and nitrogen as the driver gas

4 Experimental uncertainty

In any experimental investigation, the uncertainty assessment deals with the accuracies involved in the instruments and subsequently its effects in the global measurements as given by equation (5). The method of sequential perturbation technique has been used for uncertainty calculation (Moffat, 1985). The instruments used in the present investigations include pressure measurements through mercury manometer, digital pressure gauge and pressure transducers, transient temperature measurement through CSJT and subsequent estimation of heat flux histories. The data acquisition system involves necessary instrumentation such as power supply unit, voltage amplifier and oscilloscopes. Based on the manufacturer's specification the accuracy of these units is $\pm 0.01^\circ\text{C}$, $\pm 0.015\%$, $\pm 0.015\%$, $\pm 0.02\%$, $\pm 0.01\%$ and $\pm 0.12\%$ respectively. The uncertainty in accounting for calculation of sensitivity of CSJT was about $\pm 0.345\%$. The uncertainty analysis has been performed for calculations of shock Mach number and subsequently its effect on reflected shock Mach number, pressure and temperature ratios across primary and reflected shocks. Similarly, uncertainties for temperature measurements and heat flux calculation are also estimated during shock tube calibration. The average values of overall uncertainties for each of the parameters are given in Table 4.

$$W_R = \left[\left(\frac{\partial R}{\partial x_1} w_1 \right)^2 + \left(\frac{\partial R}{\partial x_2} w_2 \right)^2 + \dots + \left(\frac{\partial R}{\partial x_n} w_n \right)^2 \right] \quad (5)$$

where R is a given function of the independent variable $x_1, x_2, x_3, \dots, x_n$, i.e., $R = R(x_1, x_2, x_3, \dots, x_n)$ W_R is the uncertainty for the parameter R and $w_1, w_2, w_3, \dots, w_n$ are the uncertainty in the individual independent variables.

5 Conclusions

A moderate size shock tube (7 m) has been installed successfully by measuring and estimating shock tube parameters. The parametric studies are achieved through experiments and analytical calculations with an average deviation of $\pm 12\%$. For nitrogen driver, these deviations seem to be less (within $\pm 8\%$). Further, with helium driver, all the shock tube parameters are significantly high that makes it suitable for short duration application studies. Moreover, the in-house designed CSJT helps in estimating maximum rate of temperature rise and stagnation heat flux. It has been found that the maximum rate of temperature rise recorded by the current CJST, during step change in temperature for a very short duration, is around 7,800 K/s. This parameter is noted to be independent of magnitude of the step; since it has been regarded as property of the sensor. As a consequence of this fact, the nature of the heat flux signal in all the experiments is found to be similar. Further, shock tube is recommended for evaluating this constant parameter of any thermal sensor, since it can provide the necessary high temperature bath of any magnitude for a very short duration. All experimental data are accurate in the uncertainty level of $\pm 9\%$. Most of the components and instrumentations of this shock tube are indigenously designed and fabricated. The strengths of shock waves can be substantially increased by employing driver gases with lower molecular weights (such as helium) and thicker diaphragms. Shock tube as a momentary hot temperature bath for calibration high-speed thermal sensors, momentary pressure reservoir to study deformation behaviour on structures and materials are some of the important aspects of interdisciplinary studies. Being modular in nature, the future scope of this facility development is inclined towards many interesting mechanical applications in the areas of impact assessment on structures and shock assisted deformation studies on generic models, chemical kinetics, ignition delay measurements for potential biofuels.

References

- Agarwal, S., Sahoo, N., Irimpan, K.J., Menezes, V. and Desai, S. (2017) 'Comparative performance assessments of surface junction probes for stagnation heat flux estimation in a hypersonic shock tunnel', *International Journal of Heat and Mass Transfer*, Vol. 114, pp.748–757.
- Anderson, J.D. Jr. (2004) *Modern Compressible Flow with Historical Perspective*, 3rd ed., McGraw-Hill, New York.
- Andreotti, R., Colombo, M., Guardone, A., Martinelli, P., Riganti, G. and Di Prisco, M. (2015) 'Performance of a shock tube facility for impact response of structures', *International Journal of Non-Linear Mechanics*, Vol. 72, pp.53–66.
- Bhaskaran, K. and Roth, P. (2002) 'The shock tube as wave reactor for kinetic studies and material systems', *Progress in Energy and Combustion Science*, Vol. 28, No. 2, pp.151–192.
- Cobb, H.M. (2010) *The History of Stainless Steel*, ASM International.
- Doolan, C.J. and Morgan, R.G. (1999) 'A two-stage free piston driver', *Shock Waves*, Vol. 9, pp.239–243.
- Duff, R.E. and Blackwell, A.N. (1966) 'Explosive driven shock tubes', *Review of Scientific Instruments*, Vol. 37, No. 5, pp.579–586.

- Itoh, K., Komuro, T., Sato, K., Tanno, H. and Ueda, S. (2001) 'Hypersonic aerodynamic research of HOPE using high enthalpy shock tunnel', *AIAA 10th International Space Planes and Hypersonic systems and Technologies Conference*, pp.24–27, April, Kyoto, Japan.
- Kore, R., Waychal, A., Agarwal, S., Yadav, P., Uddin, A., Sahoo, N. and Shelke, A. (2016) 'Impact induced solitary wave propagation through a woodpile structure', *Smart Materials and Structures*, Vol. 25, No. 2, pp.025–027.
- Menezes, V. and Bhat, S. (2010) 'A coaxial thermocouple for shock tunnel applications', *Review of Scientific Instruments*, Vol. 81, No. 10, pp.104905–104909.
- Modarres, D. and Azzazy, M. (1988) 'Modern experimental techniques for high speed flow measurements', *AIAA, 26th Aerospace Sciences Meeting*, Nevada.
- Moffat, R.J. (1985) 'Using uncertainty analysis in planning of an experiment', *ASME J. Fluids Engineering*, Vol. 107, pp.173–178.
- Mohammed, H., Salleh, H. and Yusoff, M.Z. (2008) 'Design, fabrication of coaxial surface junction thermocouples for transient heat transfer measurements', *International Communication of Heat and Mass Transfer*, Vol. 35, No. 7, pp.853–859.
- Nanda, S.R., Agarwal, S., Kulkarni, V. and Sahoo, N. (2017) 'Shock tube as an impulsive application device', *International Journal of Aerospace Engineering*.
- Persico, G., Gaetani, P. and Guardone, A. (2005) 'Dynamic calibration of fast-response probes in low-pressure shock tubes', *Measurement Science and Technology*, Vol. 16, No. 9, pp.17–51.
- Ray, N., Jagadeesh, G. and Suwas, S. (2015) 'Response of shock wave deformation in AA5086 aluminum alloy', *Materials Science and Engineering A*, Vol. 622, pp.219–227.
- Schultz, D.L. and Jones, T.V. (1973) *Heat Transfer Measurements in Short Duration Hypersonic Facilities*, AGARD-AG-165.
- Spadaccini, L.J. and Colket, M.B. (1994) 'Ignition delay characteristics of methane fuels', *Progress in Energy and Combustion Science*, Vol. 20, No. 5, pp.431–460.
- Stalker, R.J., Paull, A., Mee, D.J., Morgan, R.G. and Jacobs, P.A. (2005) 'Scramjets and shock tunnels – the Queensland experience', *Progress in Aerospace Sciences*, Vol. 41, pp.471–513.
- Takayama, K., Reddy, K.P.J. and Kumar, C.S. (2014) *Shock Waves Made Simple*, Wiley India Pvt. Ltd., India.
- Taler, J. (1996) 'Theory of transient experimental techniques for surface heat transfer', *Int. J. Heat Mass Transfer*, Vol. 39, pp.3733–3748.
- Timoshenko, S., Timoshenko, S.P., Timoshenko, S.P. and Timoshenko, S.P. (1956) *Strength of Materials*, Vol. 210, Van Nostrand, New York.